Diabetologia (2018) 61:881–895
https://doi.org/10.1007/s00125-017-4523-9

ARTICLE

Both conditional ablation and overexpression of E2 SUMO-conjugating enzyme (UBC9) in mouse pancreatic beta cells result in impaired beta cell function

Xiaoyu He[1] · Qiaohong Lai[1] · Cai Chen[1] · Na Li[1] · Fei Sun[1] · Wenting Huang[1] · Shu Zhang[1] · Qilin Yu[1] · Ping Yang[1] · Fei Xiong[1] · Zhishui Chen[1] · Quan Gong[2] · Boxu Ren[2] · Jianping Weng[3] · Décio L. Eizirik[4] · Zhiguang Zhou[5] · Cong-Yi Wang[1]

Received: 1 August 2017 / Accepted: 16 November 2017 / Published online: 3 January 2018

Abstract

Aims/hypothesis Post-translational attachment of a small ubiquitin-like modifier (SUMO) to the lysine (K) residue(s) of target proteins (SUMOylation) is an evolutionary conserved regulatory mechanism. This modification has previously been demonstrated to be implicated in the control of a remarkably versatile regulatory mechanism of cellular processes. However, the exact regulatory role and biological actions of the E2 SUMO-conjugating enzyme (UBC9)-mediated SUMOylation function in pancreatic beta cells has remained elusive.

Methods Inducible beta cell-specific *Ubc9* (also known as *Ube2i*) knockout (KO; $Ubc9^{\Delta beta}$) and transgenic ($Ubc9^{Tg}$) mice were employed to address the impact of SUMOylation on beta cell viability and functionality. *Ubc9* deficiency or overexpression was induced at 8 weeks of age using tamoxifen. To study the mechanism involved, we closely examined the regulation of the transcription factor nuclear factor erythroid 2-related factor 2 (NRF2) through SUMOylation in beta cells.

Results Upon induction of *Ubc9* deficiency, $Ubc9^{\Delta beta}$ islets exhibited a 3.5-fold higher accumulation of reactive oxygen species (ROS) than $Ubc9^{f/f}$ control islets. Islets from $Ubc9^{\Delta beta}$ mice also had decreased insulin content and loss of beta cell mass after tamoxifen treatment. Specifically, at day 45 after *Ubc9* deletion only 40% of beta cell mass remained in $Ubc9^{\Delta beta}$ mice, while 90% of beta cell mass was lost by day 75. Diabetes onset was noted in some $Ubc9^{\Delta beta}$ mice 8 weeks after induction of *Ubc9* deficiency and all mice developed diabetes by 10 weeks following tamoxifen treatment. In contrast, $Ubc9^{Tg}$ beta cells displayed an increased antioxidant ability but impaired insulin secretion. Unlike $Ubc9^{\Delta beta}$ mice, which spontaneously developed diabetes, $Ubc9^{Tg}$ mice preserved normal non-fasting blood glucose levels without developing diabetes. It was noted that SUMOylation of NRF2 promoted its nuclear expression along with enhanced transcriptional activity, thereby preventing ROS accumulation in beta cells.

Conclusions/interpretation SUMOylation function is required to protect against oxidative stress in beta cells; this mechanism is, at least in part, carried out by the regulation of NRF2 activity to enhance ROS detoxification. Homeostatic SUMOylation is also likely to be essential for maintaining beta cell functionality.

Xiaoyu He and Qiaohong Lai contributed equally to this study.

Electronic supplementary material The online version of this article (https://doi.org/10.1007/s00125-017-4523-9) contains peer-reviewed but unedited supplementary material, which is available to authorised users.

✉ Cong-Yi Wang
wangcy@tjh.tjmu.edu.cn

✉ Zhiguang Zhou
zhouzg@hotmail.com

[1] The Center for Biomedical Research, Key Laboratory of Organ Transplantation, Ministry of Education and Ministry of Health, Tongji Hospital, Tongji Medical College, Huazhong University of Science and Technology, 1095 Jiefang Avenue, Wuhan 430030, People's Republic of China

[2] Medical College of Yangtze University, Jingzhou, Hubei, People's Republic of China

[3] Department of Endocrinology and Metabolism, The Third Affiliated Hospital, Sun Yat-Sen University, Guangzhou, People's Republic of China

[4] ULB Center for Diabetes Research, Université Libre de Bruxelles, Brussels, Belgium

[5] Diabetes Center, The Second Xiangya Hospital, Institute of Metabolism and Endocrinology, Central South University, Changsha 410011, People's Republic of China

Research in context

What is already known about this subject?

- SUMOylation regulates the viability of pancreatic beta cells
- SUMOylation is a novel signalling pathway in the regulation of insulin secretion
- A number of SUMO-modified proteins are present in the nucleus and play a crucial role in the regulation of insulin gene expression in beta cells

What is the key question?

- What is the exact global role of SUMOylation in pancreatic beta cell survival and function?

What are the new findings?

- By targeting the E2 SUMO-conjugating enzyme (UBC9; the only conjugating enzyme essential for the SUMO system), we generated mouse models of diabetes with pancreatic beta cell-specific inducible depletion or enhancement of SUMOylation function
- Remarkably, all mice developed diabetes after induction of beta cell *Ubc9* deficiency
- Interestingly, the beta cell-specific *Ubc9* transgenic mouse model ($Ubc9^{Tg}$), which does not develop spontaneous diabetes, manifested abnormal glucose tolerance coupled with impaired beta cell insulin secretion following induced *Ubc9* overexpression

How might this impact on clinical practice in the foreseeable future?

- Targeting of the SUMOylation and deSUMOylation pathway may provide a novel therapeutic option for the treatment of type 1 diabetes

Keywords Diabetes · Insulin content · Insulin secretion · NRF2 · Oxidative stress · Pancreatic beta cell · SUMOylation · UBC9

Abbreviation

ARE	Antioxidant response element
ChIP	Chromatin immunoprecipitation
CHX	Cycloheximide
DCFH-DA	2′,7′-Dichlorodihydrofluorescein diacetate
EMSA	Electrophoretic mobility shift assay
HA	Haemagglutinin
KO	Knockout
mu	Mutated
NAC	N-acetylcysteine
NRF2	Nuclear factor erythroid 2-related factor 2
NTg	Tamoxifen-induced *Ubc9* transgenic mouse model (controls)
ROS	Reactive oxygen species
SENP1	Sentrin-specific protease 1
STZ	Streptozocin
SUMO	Small ubiquitin-like modifier
UBC9	E2 SUMO-conjugating enzyme
$Ubc9^{\Delta beta}$	Beta cell-specific *Ubc9* knockout mouse model
$Ubc9^{CAT\text{-}Tg}$	Inducible *Ubc9* transgenic mouse model
$Ubc9^{f/f}$	$Ubc9^{flox}$ mice
$Ubc9^{Tg}$	Beta cell-specific *Ubc9* transgenic mouse model
WT	Wild-type

Introduction

Post-translational attachment of a small ubiquitin-like modifier (SUMO) to the lysine (K) residue(s) of a target protein (defined as SUMOylation) is an evolutionarily conserved regulatory mechanism. Studies over the past two decades have demonstrated that SUMOylation is a remarkably versatile regulatory mechanism of protein function with implications for signal transduction, gene transcription, maintenance of genome stability, protein targeting, tumourigenesis and glucose metabolism [1–3]. Previous studies including our own have demonstrated that SUMOylation regulates the viability of pancreatic beta cells [4–15]. A number of studies suggested that SUMO-modified proteins were present in the nucleus and played a crucial role in the regulation of insulin gene expression in beta cells [7–9]. Subsequent data extended

SUMOylation's function outside the nucleus [10–12, 14–16], indicating SUMOylation as a novel signalling pathway in the regulation of insulin secretion. More recently, SUMO1 has been considered as a novel antiapoptotic protein in islets, as upregulation of sentrin-specific protease 1 (SENP1), a SUMO deconjugation enzyme, reduced cell viability, resulting in impaired islet function [4]. However, studies involving islet-specific *Senp1* deletion in mice further noted that loss of *Senp1* impaired amplification of insulin exocytosis [13]. To address the exact role of SUMOylation in pancreatic beta cell survival and function, we generated mouse models of diabetes with inducible depletion or enhancement of SUMOylation function specifically in pancreatic beta cells by targeting E2 SUMO-conjugating enzyme (UBC9), the only conjugating enzyme essential for the SUMO system.

Methods

Animals The *Ubc9* (also known as *Ube2i*)^{flox} (*Ubc9*$^{f/f}$) mice were generated as detailed in Fig. 1a. The Rip-CreER (Cre) mice, which were kindly provided by D. Melton (Harvard University, MA, USA), express Cre recombinase under the control of the rat insulin 2 promoter. The Flp transgenic mice were purchased from the Jackson's Laboratory (Bar Harbor, ME, USA). The inducible *Ubc9* transgenic mouse model (*Ubc9*$^{CAT\text{-}Tg}$) was created by inserting the *Ubc9* coding sequence into a pCAG-CAT-X vector, which was provided by Q. Yang (University of Alabama at Birmingham, AL, USA). All mice had been backcrossed onto the C57BL/6 background for ten generations. The *Ubc9*$^{f/f}$ and *Ubc9*$^{CAT\text{-}Tg}$ mice were next crossed with Cre mice, and beta cell-specific *Ubc9* deficiency or overexpression was induced at 8 weeks of age using tamoxifen (75 mg/kg; Sigma, St Louis, MO, USA) intraperitoneally for 5 consecutive days. All experimental mice were treated with tamoxifen in the same protocol. Analyses were performed starting 7 days after the final tamoxifen injection. Cre-mediated excision of *Ubc9* was assessed by PCR using genomic DNA derived from pancreatic islets with the primers 5′-ACC TGG ATC TTG CCC TCC TT- 3′ and 5′-CAG CTC AGA CCT GGC CTT ACT-3′.

In all animal studies, male mice were used and littermates were served as control animals. Mice were housed individually in ventilated cages in a pathogen-free facility with a 12 h light/dark cycle, and were fed with a standard mouse chow diet. All procedures involving animals were approved by the Tongji Hospital Animal Care and Use Committee in accordance with the National Institutes of Health (NIH) guidelines.

Streptozocin induction, *N*-acetylcysteine treatment and monitoring of blood glucose level The mice were stressed by multiple low doses of streptozocin (STZ; 50 mg/kg per day for 4 consecutive days) as previously reported [17]. Treatments with 0.1% (wt/vol.) *N*-acetylcysteine (NAC) (Beyotime, Shanghai, China) were begun at day 7 after tamoxifen treatment. The mice were considered to have developed diabetes once non-fasting blood glucose levels exceeded 13.9 mmol/l for 2 consecutive days (see ESM Methods).

Intraperitoneal glucose and insulin tolerance test and islet insulin measurements Intraperitoneal glucose and insulin tolerance tests were undertaken as previously described [18]. Pancreatic islet isolation, insulin secretion assay and islet insulin content measurement were carried out using established techniques [18, 19]. Analysis of insulin concentration was performed using a Rat/Mouse Insulin ELISA kit (Millipore, Billerica, MA, USA) (see ESM Methods).

Histological and histochemical analysis, and TUNEL assay Pancreases were subjected to H&E staining [20], immunohistochemical staining (UBC9, insulin and glucagon) [21], immunofluorescence staining (insulin, glucagon and cleaved caspase-3) [22], and TUNEL assay [23] as reported (see ESM Methods). Isolated islets were visualised by electronic microscopy.

Real-time RT-PCR and western blot analysis

Real-time RT-PCR [24] was used to determine the mRNA expression levels of antioxidant genes (*Sod1*, *Sod2*, *Gpx1*, *Gstp1*, *Cat*, *Txnrd1*, *Ho-1* [also known as *Hmox1*], *Nqo1*). *Gapdh* was used for normalisation. The primer sequences for all examined genes are listed in ESM Table 1. Protein levels of UBC9, SUMO1, nuclear factor erythroid 2-related factor 2 (NRF2), ubiquitin and haemagglutinin (HA) were analysed by western blot analysis as previously described [25] (see ESM Methods).

Analysis of ROS levels The levels of reactive oxygen species (ROS) in the islets under physiological conditions were determined by analysis of islet lysates using a mouse ROS ELISA kit (Lanpai, Shanghai, China). The isolated islets and NIT-1 cells were stimulated with 2.5 mmol/l or 10 mmol/l STZ, respectively. ROS accumulation was analysed using 2′,7′-dichlorodihydrofluorescein diacetate (DCFH-DA, 10 μmol/l; Beyotime, Shanghai, China) as previously described [26] (see ESM Methods).

Plasmid constructs and transfection Expression plasmids for full-length *Nrf2* (also known as *Nfe2l2*), *Ubc9*, *Sumo1* and relative mutations were constructed as previously described [27] (see ESM Methods). NOD-derived NIT-1 cells and human embryonic kidney (HEK) 293 cells were transferred from the Center for Biotechnology and Genomic Medicine, Georgia Regents University (now named Augusta

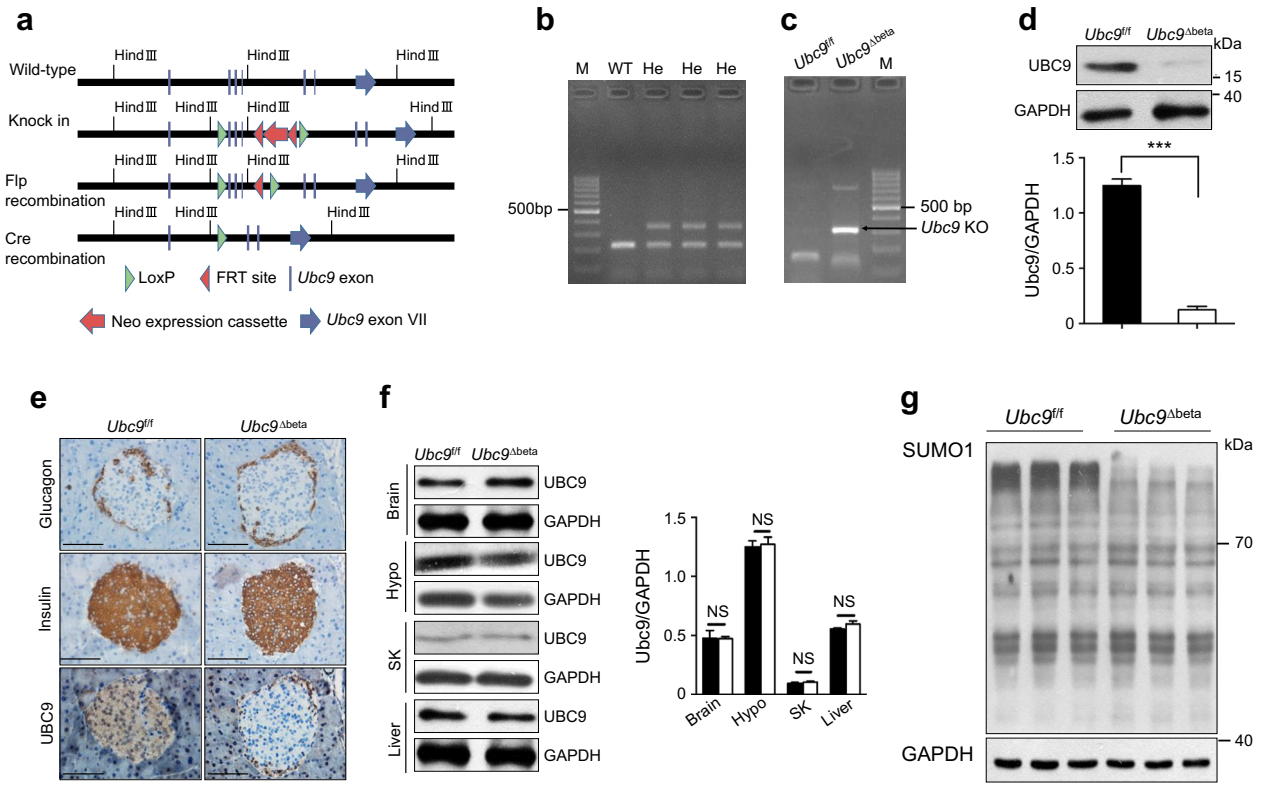

Fig. 1 Establishment of an inducible beta cell-specific *Ubc9* KO (*Ubc9*$^{\Delta beta}$) mouse model. (**a**) Strategy for generating a conditional *Ubc9*-deficient model. *Ubc9* exons 2–4 were flanked by a neo-flippase recognition target (FRT) and two loxP sites. The neo-gene was deleted after Flp recombination and the *Ubc9* exons were then excised by Cre recombinase. (**b**) PCR analysis of the neo-FRT allele. He, heterozygote; M, marker. (**c**) PCR analysis of genomic islet DNA derived from *Ubc9*$^{f/f}$ and *Ubc9*$^{\Delta beta}$ mice. (**d**) Western blot analysis of UBC9 production in islets isolated from *Ubc9*$^{f/f}$ and *Ubc9*$^{\Delta beta}$ mice, and a bar graph showing data derived from three mice in each group. Black bar, *Ubc9*$^{f/f}$; white bar, *Ubc9*$^{\Delta beta}$. (**e**) Results of serial immunohistochemical staining of pancreatic sections. Three serial sections from *Ubc9*$^{f/f}$ and *Ubc9*$^{\Delta beta}$ mice were stained for glucagon, insulin and UBC9, respectively. Scale bar, 50 μm. (**f**) Assessment of non-specific loss of *Ubc9* in various tissues in *Ubc9*$^{\Delta beta}$ mice and quantitative histogram, (n=3 mice in each group). Hypo, hypothalamus; SK, skeletal muscle. Black bars, *Ubc9*$^{f/f}$; white bars, *Ubc9*$^{\Delta beta}$. (**g**) Western blot analysis of SUMOylated proteins in islet lysates derived from *Ubc9*$^{f/f}$ and *Ubc9*$^{\Delta beta}$ mice. Glyceraldehyde 3-phosphate dehydrogenase (GAPDH) was used as internal control. The mice were killed on day 7 after tamoxifen treatment, and three mice were analysed in each group. ***p<0.001

University, Augusta, ME, USA). The cell lines were routinely tested and authenticated negative for mycoplasma contamination. Cells were transfected with the above prepared plasmids using the Lipofectamine 3000 reagent (Invitrogen, Irvine, CA, USA), and harvested for analysis 48 h after transfection.

NRF2 SUMOylation analysis Immunoprecipitation with NIT-1 cell lysate was performed to analyse endogenous SUMOylated NRF2. An in vivo SUMOylation assay and a UBC9 fusion-directed SUMOylation (UFDS) system [28] were employed to analyse the NRF2 SUMOylation sites (see ESM Methods).

Analysis of NRF2 protein stability The protein stability of NRF2 was analysed using cycloheximide (CHX) pulse-chase experiments and in vivo ubiquitination assay, as described in ESM Methods.

Analysis of NRF2 protein activity Chromatin immunoprecipitation (ChIP) assay [18], electrophoretic mobility shift assay (EMSA) [26] and dual-luciferase assay [18] were performed to analyse the activity of NRF2 (see ESM Methods).

Statistical analysis Data were expressed as means ± SEM. All statistical analyses were carried out using the Graphpad Prism 5.0 software (La Jolla, CA, USA). The data were analysed using Student's t test or one-way or two-way ANOVA where appropriate. Log-rank (Mantel–Cox) tests were employed to analyse the incidence of diabetes. In all cases, $p < 0.05$ was considered as statistically significant.

Results

Establishment of beta cell-specific UBC9-deficient model We used the strategy shown in Fig. 1a to generate a conditional *Ubc9* KO model. Three chimeric mice were obtained by genotyping the neo-flippase recognition target (FRT) allele (Fig. 1b), which was then depleted by crossing these mice

with the *Flp* (also known as *Hpd*) transgenic mice. Next, the *Ubc9*$^{f/f}$ mice were crossed with Cre mice to generate *Ubc9*$^{f/f}$-Rip-CreER mice, in which tamoxifen was used to generate beta cell-specific *Ubc9* KO (*Ubc9*$^{\Delta beta}$) mice. *Ubc9*$^{f/f}$ mice induced with tamoxifen served as control animals. The mice were killed at day 7 after tamoxifen treatment to confirm *Ubc9* deficiency. PCR analysis of islet DNA detected the KO allele, which was absent in the *Ubc9*$^{f/f}$ mice (Fig. 1c), and western blot analysis of islet lysates confirmed a significant reduction in UBC9 protein production in the *Ubc9*$^{\Delta beta}$ mice (Fig. 1d). Furthermore, serial pancreatic section immunohistochemical staining indicated that UBC9 deficiency only occurred in beta cells in *Ubc9*$^{\Delta beta}$ islets (Fig. 1e). Additionally, western blot analysis of tissue lysates from brain, hypothalamus, skeletal muscle and liver failed to detect significant differences in terms of UBC9 level between *Ubc9*$^{\Delta beta}$ and *Ubc9*$^{f/f}$ mice (Fig. 1f). Consistent with this, western blot analysis of islet lysates with a SUMO1 antibody confirmed a significant reduction in SUMOylated proteins in the *Ubc9*$^{\Delta beta}$ islets (Fig. 1g).

Mice with beta cell-specific UBC9 deficiency spontaneously develop diabetes To determine the functional impact of UBC9-mediated SUMOylation on pancreatic beta cells, we monitored blood glucose levels in *Ubc9*$^{\Delta beta}$ mice. *Ubc9*$^{f/f}$ and Cre mice induced with tamoxifen served as control animals. By day 9 after tamoxifen treatment, the *Ubc9*$^{\Delta beta}$ mice were already showing abnormal glucose tolerance, in spite of preservation of normal basal glycaemia (Fig. 2a). In line with these observations, a reduction in serum insulin levels was noted 30 min after glucose treatment in *Ubc9*$^{\Delta beta}$ mice (Fig. 2b). *Ubc9*$^{\Delta beta}$ mice maintained normal basal glucose levels up to 6 weeks following tamoxifen treatment, after which there was a progressive increase in blood glucose levels (Fig. 2c). Onset of

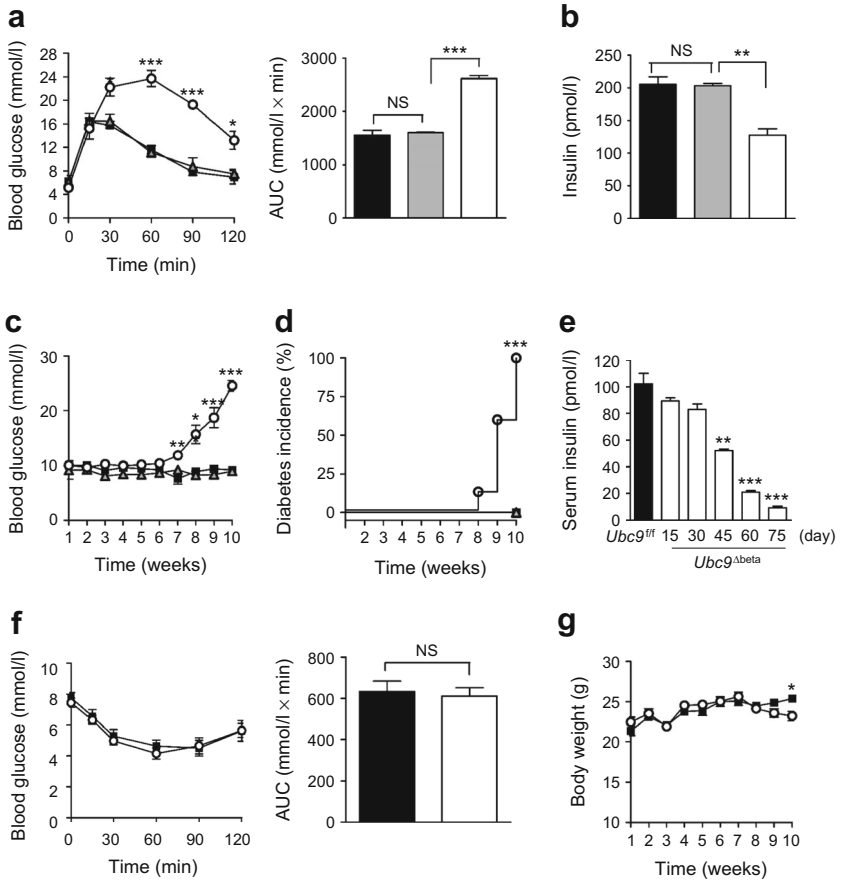

Fig. 2 *Ubc9*$^{\Delta beta}$ mice show abnormal blood glucose levels and develop spontaneous diabetes. (**a**) Blood glucose levels during IPGTT and AUC in *Ubc9*$^{f/f}$ (n=8), Cre (n=6) and *Ubc9*$^{\Delta beta}$ (n=12) mice at day 9 after tamoxifen treatment. (**b**) Plasma insulin levels determined 30 min after glucose injection during GTTs in *Ubc9*$^{f/f}$ (n=8), Cre (n=6) and *Ubc9*$^{\Delta beta}$ (n=10) mice. (**c**) Non-fasting blood glucose concentrations in *Ubc9*$^{f/f}$, Cre and *Ubc9*$^{\Delta beta}$ mice after tamoxifen treatment (n=15 for each group). (**d**) Diabetes incidence curves for *Ubc9*$^{f/f}$, Cre and *Ubc9*$^{\Delta beta}$ mice after tamoxifen treatment (n=15 for each group). (**e**) Plasma insulin levels in *Ubc9*$^{f/f}$ and *Ubc9*$^{\Delta beta}$ mice at different time points after tamoxifen treatment (n=3 for each group at each time point). (**f**) Blood glucose during intraperitoneal insulin tolerance tests and AUC in *Ubc9*$^{f/f}$ (n=8) and *Ubc9*$^{\Delta beta}$ mice (n=8) at day 15 after tamoxifen treatment. (**g**) Body weight changes for *Ubc9*$^{f/f}$ and *Ubc9*$^{\Delta beta}$ mice after tamoxifen treatment (n=15 for each group). Black squares and bars, *Ubc9*$^{f/f}$; grey triangles and bars, Cre; white circles and bars, *Ubc9*$^{\Delta beta}$. *p<0.05, **p<0.01, ***p<0.001

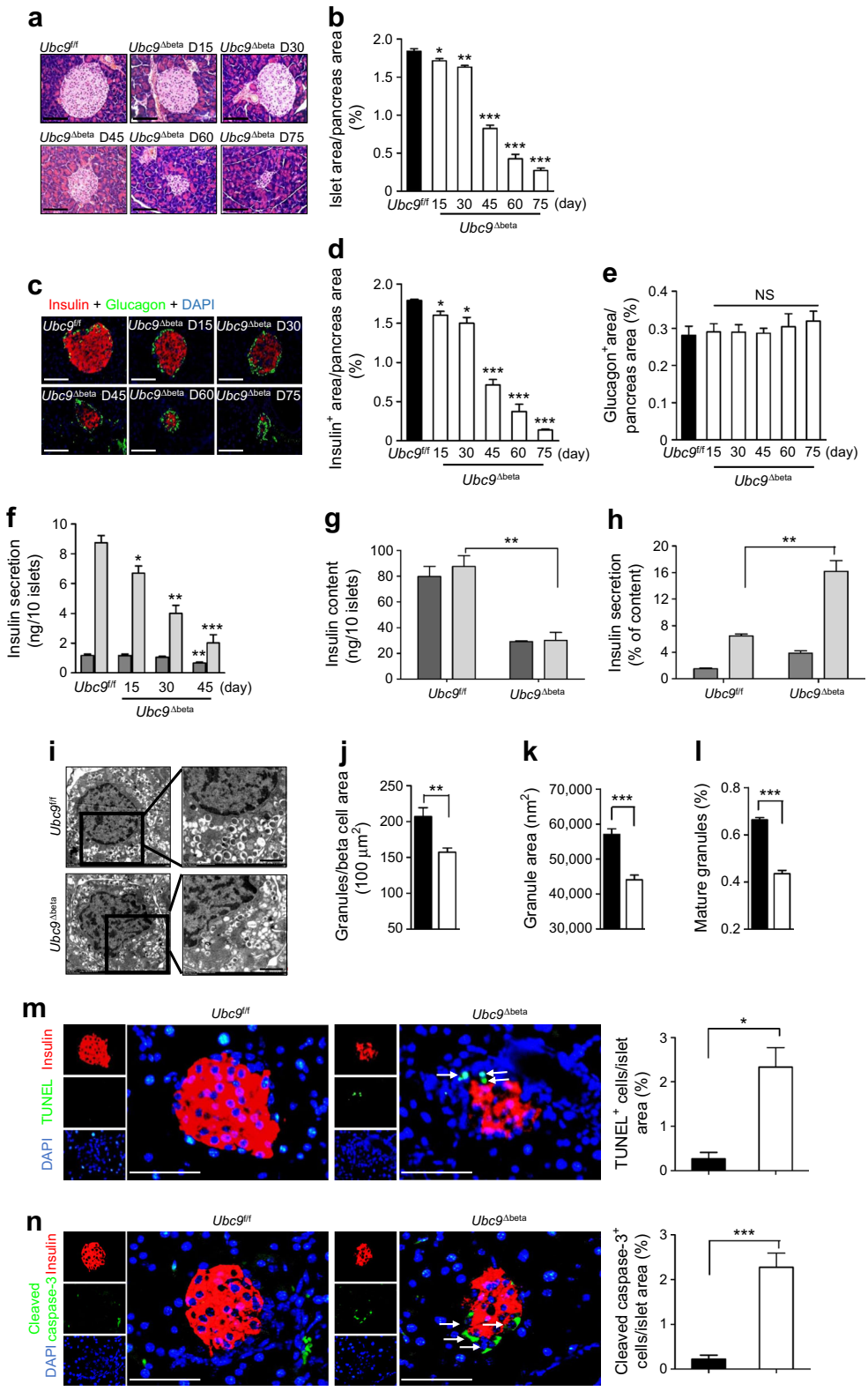

diabetes was noted in some of the *Ubc9*$^{\Delta beta}$ mice 8 weeks after tamoxifen treatment, and all mice developed diabetes by 10 weeks following tamoxifen treatment (Fig. 2d). The tamoxifen-treated *Ubc9*$^{\Delta beta}$ mice showed in parallel a progressive decrease in serum insulin levels (Fig. 2e), but preserved normal insulin sensitivity (Fig. 2f). A reduction in body weight was found 10 weeks after tamoxifen treatment, in parallel with the increase in incidence of diabetes (Fig. 2g).

◀ **Fig. 3** *Ubc9*$^{\Delta beta}$ mice show progressive beta cell loss along with reduced insulin content and beta cell apoptosis. (**a**,**b**) H&E staining of pancreatic sections and quantification of islet area in *Ubc9*$^{f/f}$ and *Ubc9*$^{\Delta beta}$ mice after tamoxifen treatment (n=5 for each group). Scale bar, 50 μm. D, Day. (**c**–**e**) Co-immunofluorescence staining of insulin and glucagon in pancreatic sections and quantification of insulin- or glucagon-positive area in *Ubc9*$^{f/f}$ and *Ubc9*$^{\Delta beta}$ mice after tamoxifen treatment (n=5 for each group). Scale bar, 50 μm. D, day. (**f**) Analysis of glucose-induced insulin release in islets isolated from *Ubc9*$^{f/f}$ and *Ubc9*$^{\Delta beta}$ mice after tamoxifen treatment. Insulin secretion rate was normalised per ten islets (n=5 mice in each group). (**g**) Insulin content of islets isolated from *Ubc9*$^{f/f}$ and *Ubc9*$^{\Delta beta}$ mice was measured at day 15 after tamoxifen treatment. (**h**) Ratio of secreted insulin at day 15 (**f**) to insulin content (**g**) represented as a percentage. (**i**) Representative results for electron microscopy of beta cells in islets isolated from *Ubc9*$^{f/f}$ (n=4) and *Ubc9*$^{\Delta beta}$ (n=5) mice. Scale bar, 1 μm. (**j**) The number of insulin granules was counted in the electron micrographs in *Ubc9*$^{f/f}$ (n=24) and *Ubc9*$^{\Delta beta}$ (n=17) beta cells. Numbers are presented as per 100 μm^2. (**k**) Quantification of insulin granule area in the electron micrographs for *Ubc9*$^{f/f}$ granules (n=121) and *Ubc9*$^{\Delta beta}$ granules (n=146). (**l**) Percentage of mature insulin granules corresponding to the granules in (**j**). (**m**) Representative results for TUNEL assays of islets at day 45 after tamoxifen treatment. Apoptotic beta cells are indicated by white arrows in the micrographs. Quantitative data are presented as the ratio of TUNEL-positive cells detected within the islet area analysed. n=5 for each group. Scale bar, 25 μm. (**n**) Results for analysis of cleaved caspase-3. Cleaved caspase-3-positive beta cells are indicated by white arrows in the micrographs, while quantitative data are presented as the ratio of cleaved caspase-3-positive cells detected within the examined islet area. n=5 for each group. Scale bar, 25 μm. Black bars, *Ubc9*$^{f/f}$; white bars, *Ubc9*$^{\Delta beta}$; dark grey, 3.3 mmol/l glucose; light grey, 16.7 mmol/l glucose. *p<0.05, **p<0.01, ***p<0.001

Together, those data indicate that a loss of SUMOylation function in beta cells, secondary to *Ubc9* deletion, induces the development of spontaneous diabetes.

Loss of UBC9 impairs beta cell function and induces beta cell apoptosis along with decreased beta cell mass The above results prompted us to check the impact of *Ubc9* deletion on beta cell mass and function. A reduction in beta cell mass was notable after day 15 of tamoxifen treatment, and became increasingly significant after day 30 of tamoxifen treatment, as evidenced by the smaller islet size (Fig. 3a,b) and decreased insulin staining area (Fig. 3c,d). In particular, at day 45 after tamoxifen treatment, only 40% of the beta cell mass remained in *Ubc9*$^{\Delta beta}$ mice, and 90% of the beta cell mass was lost by day 75 (Fig. 3a–d). In addition, the loss of beta cell mass was specific as there was no significant change in the glucagon-staining area (Fig. 3c,e). Consistent with the decreased beta cell mass, there was also a progressive decrease in glucose-stimulated insulin secretion (GSIS) in islets isolated from *Ubc9*$^{\Delta beta}$ mice, which was already observed by day 15 and reached a nadir by day 45 after tamoxifen treatment (Fig. 3f). We also measured islet insulin content at day 15 after tamoxifen treatment, with insulin content markedly lower in *Ubc9*$^{\Delta beta}$ islets than *Ubc9*$^{f/f}$ islets (Fig. 3g). However, when secreted insulin was expressed as islet insulin content, insulin secretion from *Ubc9*$^{\Delta beta}$ islets displayed a 60.1% increase compared with *Ubc9*$^{f/f}$ islets (Fig. 3h). To further evaluate whether there were ultrastructural signals of beta cell dysfunction ahead of actual beta cell loss, we used electron microscopy to examine insulin granules in islets at day 7 after tamoxifen treatment, by which time there were no differences in beta cell mass between *Ubc9*$^{\Delta beta}$ and *Ubc9*$^{f/f}$ mice (data not shown). There was a significant decrease in insulin granule volume in *Ubc9*$^{\Delta beta}$ mice compared with *Ubc9*$^{f/f}$ mice (Fig. 3i), as evidenced by the lower number (Fig. 3j) and smaller size (Fig. 3k) of the granules. Furthermore, *Ubc9*$^{\Delta beta}$ beta cells displayed a significant decline in the percentage of mature insulin granules (Fig. 3l). Taken together, our data support the fact that loss of *Ubc9* results in beta cell loss along with impaired beta cell function.

Given the observed beta cell loss in *Ubc9*$^{\Delta beta}$ mice, we investigated the presence of beta cell apoptosis. TUNEL-positive apoptotic beta cells were detected by day 30 after tamoxifen treatment in *Ubc9*$^{\Delta beta}$ islets (data not shown); this apoptosis was elevated further at day 45 following tamoxifen treatment (Fig. 3m), while apoptotic beta cells were almost undetectable in *Ubc9*$^{f/f}$ islets at all time points examined. Similarly, *Ubc9*$^{\Delta beta}$ islets displayed a significantly higher number of cleaved caspase-3-positive beta cells than did *Ubc9*$^{f/f}$ islets (Fig. 3n). Together, our data suggest that sustained loss of *Ubc9* leads to beta cell apoptosis.

Beta cells deficient in UBC9 manifest ROS accumulation and altered antioxidant capability To analyse the mechanisms by which loss of *Ubc9* leads to beta cell apoptosis, we examined ROS accumulation and antioxidant capability, as our previous studies demonstrated that SUMOylation may regulate oxidative stress in other cell types [5, 6, 29, 30]. Remarkably, far higher levels of basal ROS accumulation were noted in *Ubc9*$^{\Delta beta}$ islets than *Ubc9*$^{f/f}$ control islets (Fig. 4a). To confirm this result, we stimulated islets with STZ as described and then measured ROS accumulation by DCFH-DA staining. The *Ubc9*$^{\Delta beta}$ islets exhibited a 3.5-fold higher ROS accumulation than the *Ubc9*$^{f/f}$ control islets (Fig. 4b).

Given that rodent beta cells have low levels of antioxidant enzymes, which renders them vulnerable to oxidative damage [31–33], we next examined the levels of antioxidant enzymes following tamoxifen treatment. Notably, mRNA expression of several key antioxidant enzymes was decreased as early as day 15 after tamoxifen treatment (Fig. 4c).

NRF2 is a key transcriptional factor in the regulation of antioxidant enzymes in beta cells exposed to environmental stress [34, 35]. Interestingly, there was a nearly threefold decrease in the level of nuclear NRF2 in *Ubc9*$^{\Delta beta}$ islets compared with *Ubc9*$^{f/f}$ control islets (Fig. 4d). Consistent with this, *Ubc9*$^{\Delta beta}$ islets displayed significantly lower NRF2 binding to the response elements, as illustrated by EMSA (Fig. 4e) and ChIP assay (Fig. 4f, g). To extend these observations to in vivo

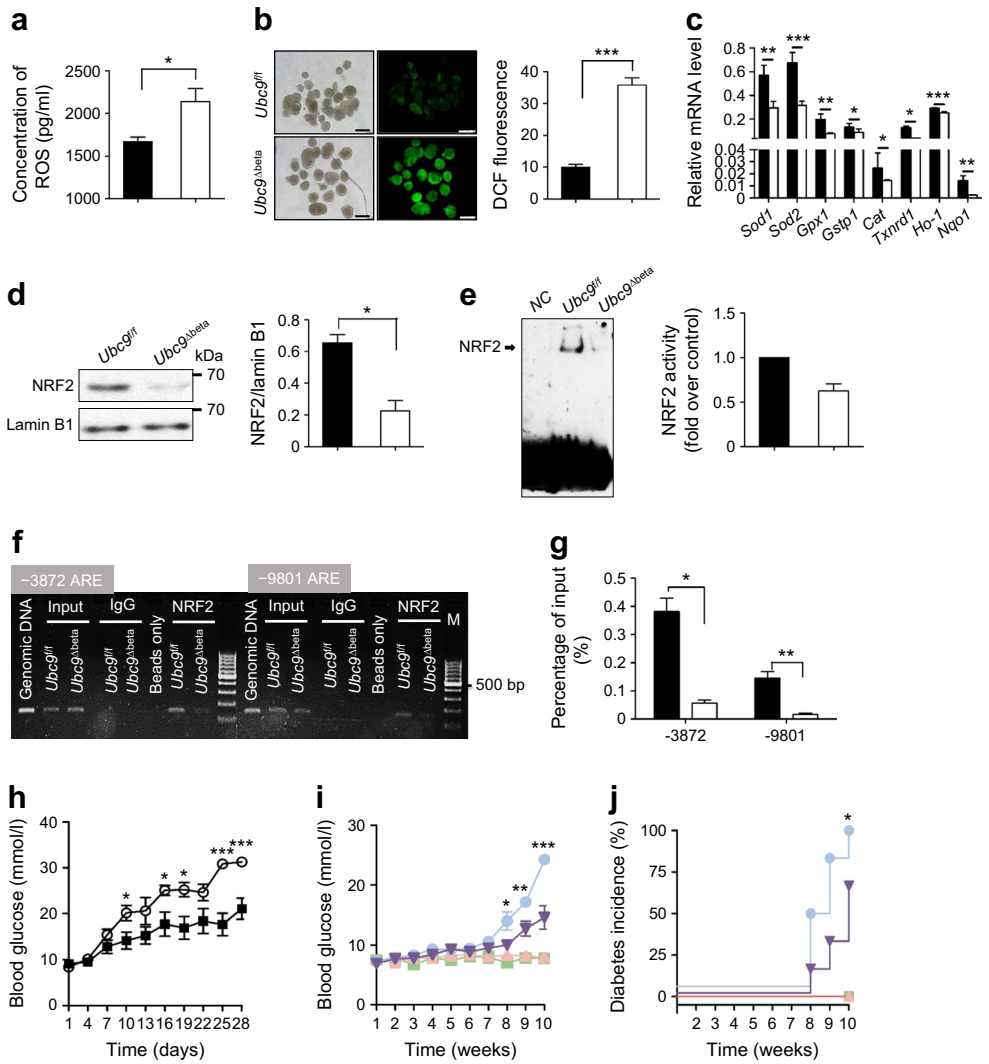

Fig. 4 *Ubc9*$^{\Delta beta}$ islets display ROS accumulation along with altered antioxidant capability. (**a**) The levels of ROS in *Ubc9*$^{f/f}$ and *Ubc9*$^{\Delta beta}$ islets 1 week after tamoxifen treatment, determined by ELISA (n=4 for each group). (**b**) ROS levels were measured by DCFH-DA staining in the islets prepared as in (**a**) that had also been treated with STZ; quantitative data are presented as DCF fluorescence intensity (n=4 for each group). Scale bar, 500 μm. (**c**) Real-time RT-PCR analysis of antioxidant genes in *Ubc9*$^{f/f}$ and *Ubc9*$^{\Delta beta}$ islets at day15 after tamoxifen treatment (n=3 for each group). (**d**) Western blot analysis of nuclear NRF2 levels in the islets at day 15 after tamoxifen treatment (n=5 mice in each group). (**e**) EMSA results for analysis of NRF2 DNA binding in *Ubc9*$^{f/f}$ and *Ubc9*$^{\Delta beta}$ islets 15 days after tamoxifen treatment. Unlabelled ARE probes served as a negative control (NC). Five hundred islets isolated from five mice for each group were used for the study, with three replications. (**f**) ChIP PCR and (**g**) real-time RT-PCR results for analysis of NRF2 binding to *HO-1* gene ARE regions in *Ubc9*$^{f/f}$ and *Ubc9*$^{\Delta beta}$ islets at day 15 after tamoxifen treatment. Five hundred islets isolated from five mice were used for the study in each group. Data shown here are representative of three similar experiments. (**h**) Non-fasting blood glucose levels in *Ubc9*$^{f/f}$ and *Ubc9*$^{\Delta beta}$ mice following multiple low doses of STZ treatment (n=15 for each group). (**i**) Non-fasting blood glucose concentrations in regular water or NAC water-fed *Ubc9*$^{f/f}$ mice (n=10 for each group) and *Ubc9*$^{\Delta beta}$ mice (n=14 for each group) after tamoxifen treatment. (**j**) Diabetes incidence curves for the mice in (**i**). Black bars and squares, *Ubc9*$^{f/f}$; white bars and circles, *Ubc9*$^{\Delta beta}$; blue line, *Ubc9*$^{\Delta beta}$ + regular water; purple line, *Ubc9*$^{\Delta beta}$+NAC water; green line, *Ubc9*$^{f/f}$+regular water; pink line, *Ubc9*$^{f/f}$+NAC water. *p<0.05, **p<0.01, ***p<0.001

situations, we exposed *Ubc9*$^{\Delta beta}$ mice (1 week after tamoxifen treatment) to multiple low doses of STZ. *Ubc9*$^{\Delta beta}$ mice were more susceptible to the STZ treatment, as evidenced by the significantly higher blood glucose levels compared with *Ubc9*$^{f/f}$ control mice (Fig. 4h). To confirm these data, we treated *Ubc9*$^{\Delta beta}$ and *Ubc9*$^{f/f}$ mice with NAC, an ROS scavenger. As expected, all regular water-fed *Ubc9*$^{\Delta beta}$ mice spontaneously developed diabetes, whereas the change in blood glucose levels was much smaller in the NAC water-fed *Ubc9*$^{\Delta beta}$ mice (Fig. 4i), in parallel with a 33% decrease in incidence of diabetes (Fig. 4j). Collectively, our data suggest that loss of *Ubc9* decreases the nuclear level and activity of NRF2, leading to deceased levels of antioxidant enzymes and thus enabling ROS accumulation in beta cells.

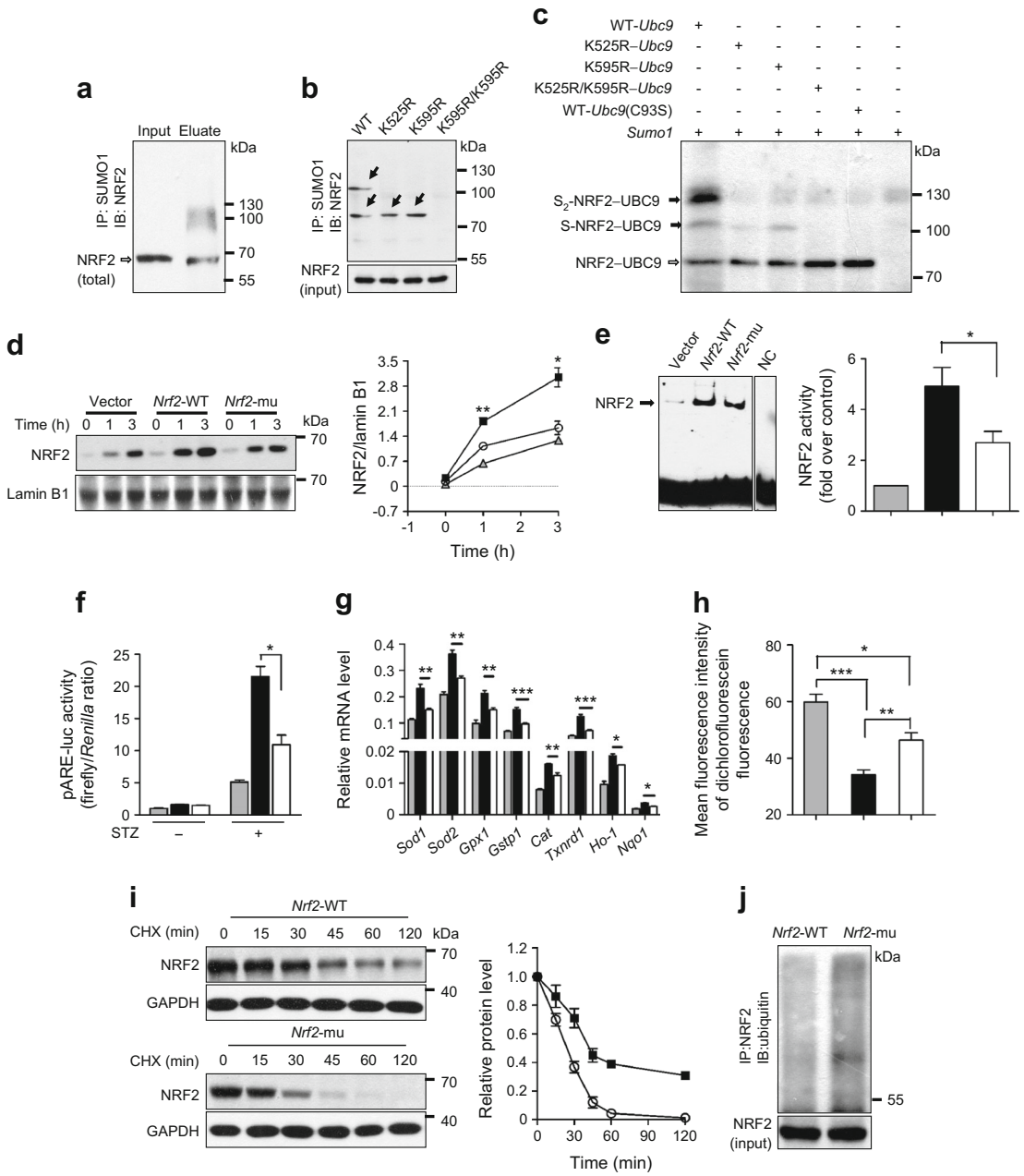

Fig. 5 SUMO1 SUMOylates NRF2 to regulate its transcriptional activity and stability. (**a**) Detection of endogenous SUMOylated NRF2 in NIT-1 cells. The SUMO1 immunoprecipitates were probed with an NRF2 antibody. (**b**) In vivo SUMOylation of NRF2. Plasmids were transfected as indicated. The SUMO1 immunoprecipitates were detected by western blotting with an NRF2 antibody. SUMOylated NRF2 is indicated by black arrows. (**c**) *Nrf2–Ubc9* fusion plasmids were co-transfected with SUMO1 as indicated, and a UBC9 antibody was used for western blot analysis of NRF2 SUMOylation. The fusion protein NRF2–UBC9 and its SUMO1 (S [or two SUMO1, S_2]) attached form are indicated. (**d**) SUMOylation increases NRF2 nuclear level. Western blot analysis of NRF2 production in the nuclear extracts of NIT-1 cells transfected with *Nrf2*-WT or *Nrf2*-mu plasmids. The line graph shows data derived from three independent experiments. (**e**) EMSA results for analysis of NRF2 DNA binding at the 3 h time point following STZ treatment. Unlabelled ARE probes served as a negative control (NC). The bar graph shows data derived from three independent experiments. (**f**) Results for luciferase reporter assays. NIT-1 cells were transfected with *Nrf2*-WT or *Nrf2*-mu plasmids, and then subjected to STZ treatment for 3 h. (**g**) Expression of antioxidant genes analysed by real-time RT-PCR in NIT-1 cells transfected with the indicated plasmids. (**h**) Flow cytometry analysis of ROS levels in DCFH-DA-stained NIT-1 cells transfected with indicated plasmids. (**i**) CHX pulse-chase treatment for analysis of the half-life of NRF2. The cells were treated with CHX for the indicated time and western blot analysis was conducted to analyse NRF2 protein levels. The line graph shows data derived from three independent experiments. (**j**) Results of an in vivo ubiquitination assay. The NRF2 immunoprecipitates were probed with an ubiquitin antibody for analysis of NRF2 ubiquitination. All studies were conducted with three replications. Grey bars and triangles, vector; black bars and squares, *Nrf2*-WT; white bars and circles, *Nrf2*-mu. IB, immunoblotting; IP, immunoprecipitation; pARE-luc, luciferase reporter gene. *$p<0.05$, **$p<0.01$, ***$p<0.001$

SUMOylation of NRF2 promotes its nuclear expression level and stability A recent study provided feasible evidence that NRF2 is a potential SUMOylation target in hepatic stellate cells [36], and our studies in NIT-1 cells (a NOD-derived beta cell line) confirmed SUMOylation of NRF2 (Fig. 5a). Different positions of NRF2 bands have been reported in diverse cell types [37–42], and the exact western blot molecular mass of NRF2 in NIT-1 cells has been verified, using an HA-tagged transfection assay, to be less than 70 kDa (ESM Fig. 1). Next, to identify the predicted SUMO1 acceptor (lysine) sites, we generated three NRF2 variants, K525R, K595R and K525R/K595R, as described. It was noted that two NRF2 reactive bands between 70 and 130 kDa could be detected in SUMO1 immunoprecipitated products originated from Nrf2 wild-type (WT) transfected NIT-1 cells, whereas only the lower reactive band could be detected in K525R or K595R transfected cells, and the SUMOylated NRF2 became undetectable once NIT-1 cells transfected with both acceptor sites mutated (K525R/K595R) (Fig. 5b). Of importance, studies in our UBC9 fusion-directed SUMOylation system produced identical results (Fig. 5c), with conduction of SUMOylation completely dependent on the catalytic activity of the fused UBC9, as WT *Nrf2* fused with active-site-mutated *Ubc9* [WT-*Ubc9*(C93S)] failed to catalyse NRF2 SUMOylation (Fig. 5c). Collectively, these data demonstrate that K525 and K595 are likely to be the only two SUMO-targeted lysine residues within NRF2, and, in our study, their SUMOylation resulted in two reactive NRF2 bands.

To address the mechanisms by which UBC9 regulates NRF2 activity, we investigated the impact of *Ubc9* deficiency on NRF2 nuclear protein level. NIT-1 cells were transfected with a WT *Nrf2* (*Nrf2*-WT) plasmid in parallel with a double SUMOylation-site-mutated (*Nrf2*-mu) plasmid, followed by STZ stimulation. We focused on the 0, 1 and 3 h time points after STZ treatment. Interestingly, *Nrf2*-WT transfected NIT-1 cells displayed around twofold higher nuclear NRF2 levels than *Nrf2*-mu transfected cells at 1 h and 3 h (Fig. 5d). In line with this result, the *Nrf2*-WT transfected NIT-1 cells manifested significantly higher NRF2 binding to the antioxidant response element (ARE) than did *Nrf2*-mu transfected cells (Fig. 5e). Importantly, luciferase reporter assays confirmed that SUMOylation of NRF2 was required for its optimal transcriptional activity (Fig. 5f). Indeed, the *Nrf2*-WT transfected cells exhibited significantly higher levels of NRF2 downstream antioxidant enzymes (Fig. 5g) along with lower levels of ROS accumulation following STZ treatment (Fig. 5h). Together, these data support the fact that SUMOylation enhances NRF2 nuclear expression, which then enhances cell capability for detoxification of ROS.

Until recently, the prevailing view was that the stability of NRF2 is regulated principally by ubiquitination and subsequent proteasomal degradation [43]. It was therefore of interest to check whether Ubc9-mediated SUMOylation would enhance NRF2 protein stability by reducing its ubiquitination. We thus conducted CHX pulse-chase studies by transfecting the *Nrf2*-WT and *Nrf2*-mu plasmids into NIT-1 cells. Remarkably, *Nrf2*-mu transfected cells were characterised by a significant decrease in NRF2 protein half-life compared with *Nrf2*-WT transfected cells (Fig. 5i), suggesting that SUMOylation may protect NRF2 from degradation. To address this question, we examined NRF2 ubiquitination in NIT-1 cells transfected as described above; the *Nrf2*-mu transfected cells did indeed display a higher level of the poly-ubiquitin-conjugated form of NRF2 than did the *Nrf2*-WT transfected cells (Fig. 5j). In addition, we constructed a plasmid expressing a constitutively active *Nrf2*-mu, which lacks the Neh2 domain of NRF2, which is responsible for binding to Kelch-like ECH-associated protein (KEAP1) [44]. Consistently, transfection of NIT-1 cells with constitutively active *Nrf2*-mu increased the stability of *Nrf2*-mu protein (ESM Fig. 2). Taken together, those data support the idea that SUMOylation stabilises NRF2 against ubiquitin-mediated proteasomal degradation.

***Ubc9*^{Tg} mice show enhanced beta cell antioxidant capacity** To investigate more deeply the role of SUMOylation in beta cell oxidative stress, we generated a loxP *Ubc9* transgenic model (*Ubc9*$^{CAT\text{-}Tg}$) as described and obtained two founders. The *Ubc9*$^{CAT\text{-}Tg}$ mice were next crossed with Cre mice as detailed in Fig. 6a. Beta cell-specific transgenic *Ubc9* expression (*Ubc9*^{Tg} mice) was induced using tamoxifen, while tamoxifen-induced *Ubc9*$^{CAT\text{-}Tg}$ mice (NTg) served as control animals. As expected, western blot analysis indicated significant transgene expression by day 7 after tamoxifen treatment in *Ubc9*^{Tg} but not in NTg mice (Fig. 6b). Consistently, western blot analysis of islet lysates with a SUMO1 antibody confirmed a significant increase in SUMOylated proteins in the *Ubc9*^{Tg} islets (ESM Fig. 3). In contrast to NTg islets, a fourfold higher nuclear level of NRF2 was noted in *Ubc9*^{Tg} islets (Fig. 6c). We then challenged *Ubc9*^{Tg} and NTg islets with STZ as described earlier. *Ubc9*^{Tg} islets displayed a nearly 2.5-fold reduction in ROS accumulation compared with NTg islets (Fig. 6d). To confirm these data, we treated *Ubc9*^{Tg} and NTg mice with multiple low doses of STZ 1 week after tamoxifen treatment. An escalating blood glucose level was noted in NTg mice after day 4 of STZ treatment, whereas the change in blood glucose level was much lower in *Ubc9*^{Tg} mice (Fig. 6e). Consistent with this, only four out of 12 *Ubc9*^{Tg} mice (33.3%) became diabetic, while 72.7% (eight out of 11) of NTg mice developed diabetes (Fig. 6f). Similarly, *Ubc9*^{Tg} mice manifested higher plasma insulin levels (Fig. 6g) and beta cell mass volume at day 24 after STZ induction (Fig. 6h). Of note, studies in another *Ubc9* transgenic line obtained consistent results (data not shown).

***Ubc9*^{Tg} mice manifest normal blood glucose level but abnormal glucose tolerance** Finally, we sought to address the

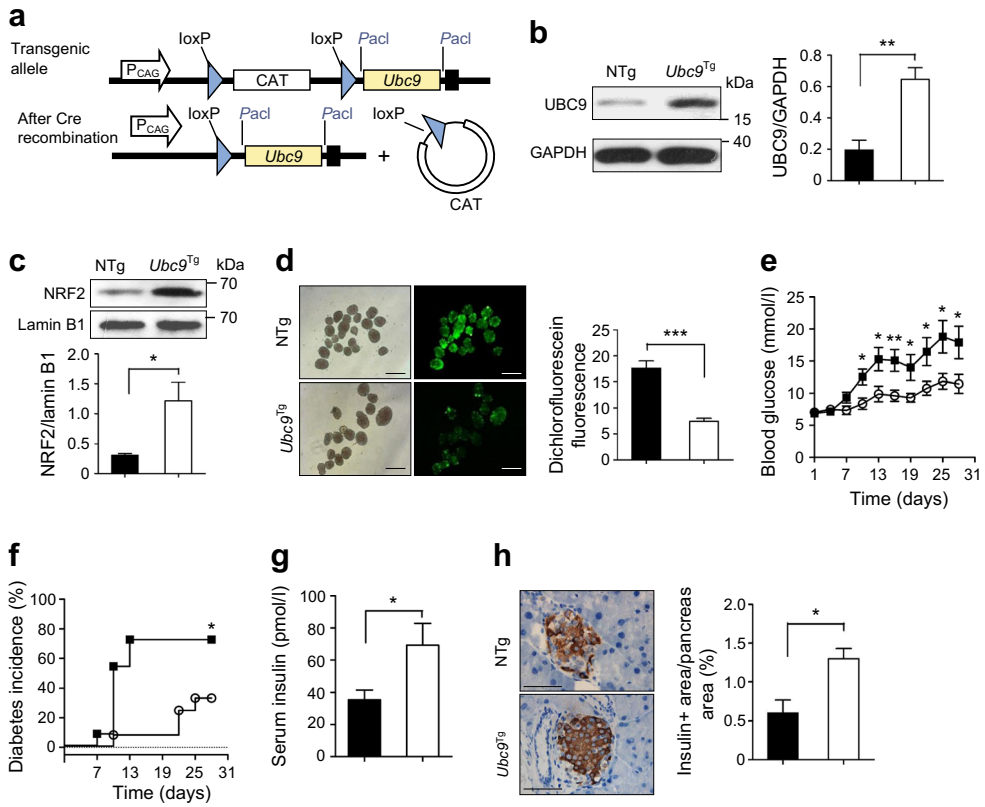

Fig. 6 $Ubc9^{Tg}$ islets manifest increased antioxidant capability. (**a**) Strategy for generating the conditional *Ubc9* transgenic mouse model. The *Ubc9* coding sequence was inserted into a pCAG-CAT-X vector, and the coding sequence of CAT was then deleted using a Cre recombinase. *P*acI, restriction enzyme; P_{CAG}, CAG promoter. (**b**) Western blot analysis of UBC9 levels in $Ubc9^{Tg}$ and control NTg islets 1 week after tamoxifen treatment. Quantitative data are also presented (three mice were analysed in each group). (**c**) Western blot analysis of nuclear NRF2 expression in NTg and $Ubc9^{Tg}$ islets on day 7 after tamoxifen treatment. The bar graph shows data derived from four animals per group. (**d**) ROS levels determined by DCFH-DA staining in NTg and $Ubc9^{Tg}$ islets. The relative levels of ROS in the islets are presented as DCF fluorescence intensity (n=4 for each group). Scale bar, 500 μm. (**e**) Non-fasting blood glucose concentration in NTg (n=11) and $Ubc9^{Tg}$ (n=12) mice following multiple low doses of STZ treatment. (**f**) Diabetes incidence curves for NTg (n=11) and $Ubc9^{Tg}$ (n=12) mice after multiple low doses of STZ treatment. (**g**) Plasma insulin levels in NTg and $Ubc9^{Tg}$ mice at day 24 after STZ administration (n=7 for each group). (**h**) Immunohistochemical staining of insulin in pancreatic sections and quantification of the insulin-positive area in NTg and $Ubc9^{Tg}$ mice at day 24 after STZ stimulation (n=5 for each group). Scale bar, 50 μm. Black bars and squares, NTg; white bars and circles, $Ubc9^{Tg}$. *p<0.05, **p<0.01, ***p<0.001

functional properties of beta cells in $Ubc9^{Tg}$ mice in the absence of exogenous STZ challenge. We noted that $Ubc9^{Tg}$ mice displayed an abnormal glucose tolerance at day 9 following induction of UBC9 transgene expression (Fig. 7a), along with a reduction in serum insulin levels 30 min after glucose stimulation (Fig. 7b). Similar to $Ubc9^{\Delta beta}$ mice, $Ubc9^{Tg}$ mice were characterised by normal insulin sensitivity (Fig. 7c). We then checked the impact of transgenic UBC9 expression on beta cell functionality. We first observed a decrease in glucose-induced insulin release compared with islets isolated from NTg mice (Fig. 7d). Next, we measured islet insulin content. Unlike insulin secretion, there was no difference between the $Ubc9^{Tg}$ and NTg islets (Fig. 7e). However, once normalised to related islet insulin content, $Ubc9^{Tg}$ islets displayed a 32.5% decrease in terms of insulin secretion compared with NTg islets (Fig. 7f). Additionally, we examined insulin granules by electron microscopy at day 15 following tamoxifen treatment. Consistent with the islet insulin content results, we failed to detect a significant difference in terms of insulin granule number (Fig. 7g,h) and size (Fig. 7g,i), or in the percentage of mature insulin granules (Fig. 7g,j), between $Ubc9^{Tg}$ and NTg mice. Based on these results, we were curious about whether $Ubc9^{Tg}$ mice would develop diabetes spontaneously, as observed in $Ubc9^{\Delta beta}$ mice. Interestingly, $Ubc9^{Tg}$ mice maintained normal glycaemia for at least 10 weeks after tamoxifen treatment, and none of them developed diabetes (Fig. 7k). Consistent with this, $Ubc9^{Tg}$ mice still preserved normal islet size (Fig. 7l) and beta cell mass volume (Fig. 7m) after 10 weeks of tamoxifen treatment. Similarly, studies in another *Ubc9* transgenic line produced consistent results (data not shown). Together, our results demonstrate that transgenic *Ubc9* impairs beta cell insulin secretion but is not associated with beta cell death, a similar phenotype to that observed in mice deficient in *Senp1* (which encodes a SUMO-deconjugating enzyme) [13].

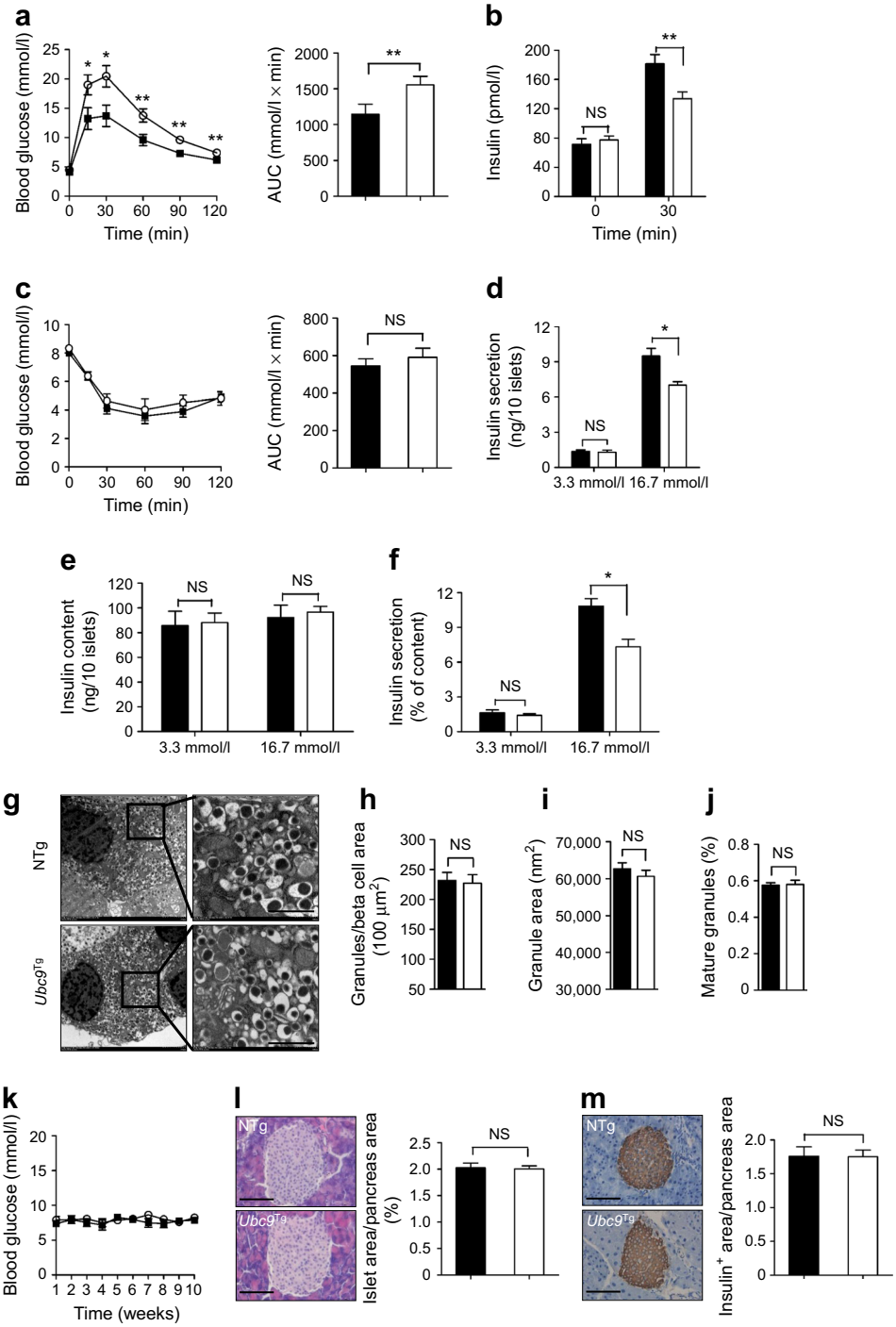

Discussion

In this study, we demonstrated that UBC9-mediated SUMOylation plays an essential role in the maintenance of beta cell survival and functionality. Beta cells deficient in *Ubc9* manifest impaired antioxidant capacity, decreased insulin content and beta cell mass loss, along with progressive alterations in glucose homeostasis and ultimately severe diabetes. Insufficient insulin supply is likely contributed to by both impaired beta cell function and excessive apoptosis, suggesting that SUMOylation function is required for the maintenance of beta cell integrity. At the molecular level, loss of *Ubc9* leads to the attenuated NRF2 activity and decreased expression of its downstream antioxidant genes, and consequently results in accumulation of ROS and oxidative stress. In support of these data, transgenic expression of UBC9 in beta cells significantly enhances their antioxidant capacity. Previous in vitro studies indicated that enhanced SUMOylation protects beta cells

◀ **Fig. 7** Characteristics of beta cells in $Ubc9^{Tg}$ mice under physiological conditions. (**a**) Blood glucose levels during IGTTs and AUC for NTg (n=15) and $Ubc9^{Tg}$ (n=16) mice at day 9 after tamoxifen treatment. (**b**) Plasma insulin levels determined 30 min after glucose injection during GTTs in NTg (n=7) and $Ubc9^{Tg}$ (n=8) mice. (**c**) Blood glucose levels during intraperitoneal insulin tolerance tests and AUC for NTg (n=8) and $Ubc9^{Tg}$ (n=9) at day 15 after tamoxifen treatment. (**d**) Analysis of glucose-stimulated insulin secretion in islets isolated from NTg and $Ubc9^{Tg}$ mice at day 15 after tamoxifen treatment. Insulin secretion rate was normalised per ten islets (n=5 mice in each group). (**e**) Insulin content of the islets in (**d**). (**f**) Ratio of secreted insulin (**d**) to insulin content (**e**) represented as a percentage. (**g**) Representative images for electron microscopy of beta cells in islets isolated from NTg (n=5) and $Ubc9^{Tg}$ (n=5) mice 15 days after tamoxifen treatment. Scale bar, 1 μm. (**h**) The number of insulin granules was counted in the electron micrographs of NTg (n=20) and $Ubc9^{Tg}$ (n=25) beta cells. The numbers are presented per 100 um^2. (**i**) Quantification of insulin granule area in the electron micrographs. NTg granules, n=250; $Ubc9^{Tg}$ granules, n=208. (**j**) Percentage of mature insulin granules corresponding to the granules in (**h**). (**k**) Non-fasting blood glucose concentrations in NTg and $Ubc9^{Tg}$ mice after tamoxifen treatment (n=15 for each group). (**l**) H&E staining of pancreatic sections and quantification of islet area in NTg and $Ubc9^{Tg}$ at week 10 after tamoxifen treatment (n=5 for each group). Scale bar, 50 μm. (**m**) Immunohistochemical staining of insulin in pancreatic sections and quantification of the insulin-positive area in NTg and $Ubc9^{Tg}$ mice at week 10 after tamoxifen treatment (n=5 for each group). Scale bar, 50 μm. NTg, black bars and squares; $Ubc9^{Tg}$, white bars and circles. *p<0.05, **p<0.01

against apoptosis, while ectopic production of SENP1, a SUMO-deconjugating enzyme, induces detrimental effects on beta cell survival [4]. Taken together, these and the present data support the notion that beta cell integrity and intracellular homeostasis relies on its SUMOylation function.

The role of NRF2 in protecting pancreatic beta cells against oxidative, nitrosative and metabolic stress has been well recognised in models of diabetes [34, 35, 45]. However, the molecular mechanisms underlying the regulation of basal NRF2 activity and the magnitude of its activation in response to diverse forms of stress in beta cells are still to be fully characterised. Previous studies in hepatic stellate cells suggest that SUMOylation at specific lysine residues is required for NRF2 ARE binding [36]. We confirmed that NRF2 is also a substrate for UBC9-mediated SUMOylation in pancreatic beta cells, and identified K525 and K595 as two SUMOylation sites for NRF2. To analyse the functional relevance of this SUMOylation, we generated an *Nrf2*-mu plasmid in which the two SUMOylation sites (lysine residues) were mutated into arginines (K525R and K595R). Subsequent studies in NIT-1 cells provided experimental evidence that SUMOylation of these two lysine residues promotes NRF2 transcriptional activity and protein stability.

Additionally, we conducted experiments using a beta cell-specific UBC9 overexpression mouse model ($Ubc9^{Tg}$) that displayed an increased antioxidant ability but impaired glucose tolerance. Analysis of islet insulin content revealed that the mechanisms underlying beta cell dysfunction in $Ubc9^{\Delta beta}$ and $Ubc9^{Tg}$ mice are likely to be very different. Indeed, beta cells originated from $Ubc9^{\Delta beta}$ mice were characterised by a significant decrease in insulin content, which probably contributed to the reduced insulin secretion. In contrast, $Ubc9^{Tg}$ beta cells preserved a normal insulin content, but showed the impaired insulin secretion. In fact, this phenotype is quite similar to that described in a previous study carried out in beta cell-specific *Senp1*-deficient mice, in which loss of *Senp1* reduced insulin exocytosis [13]. Additionally, SUMOylation also downregulates insulin secretion via glucagon-like peptide-1 (GLP-1)-regulated cAMP generation [14, 15]. Taken together, these data suggest that UBC9-mediated SUMOylation is required for pancreatic beta cell survival, but SENP1-mediated de-SUMOylation is required for beta cell insulin secretion. Therefore, a physiologically normal beta cell should maintain a dedicated homeostasis between SUMOylation and de-SUMOylation.

In summary, beta cells deficient in *Ubc9* have an altered redox equilibrium, leading to accumulation of ROS and oxidative stress. This oxidative stress impairs beta cell function, causes loss of beta cell mass and eventually leads to diabetes. Additionally, beta cells with an enhanced SUMOylation function caused by transgenic *Ubc9* expression are more resistant to oxidative stress, and our data support the notion that an enhanced SUMOylation function would improve beta cell viability against oxidative stress in spite of impaired insulin secretion in $Ubc9^{Tg}$ mice. Given that a loss of *Ubc9* would result in a global effect on beta cells, we cannot exclude the possibility that additional mechanisms, such as endoplasmic reticulum stress, also contribute to impaired beta cell function and viability. In this report, however, we only focused on the effect of NRF2 activity on altered redox homeostasis, which seems to act as a critical factor for protection of beta cells against oxidative stress. Likewise, our $Ubc9^{\Delta beta}$ and $Ubc9^{Tg}$ models will serve as useful tools to analyse the global effects of SUMOylation on beta cell survival and function, and to screen for reagents that mimic the beneficial effects of UBC9 for clinical applications.

Acknowledgements We are grateful to D. Melton (Harvard University, Cambridge, MA, USA) for providing the Rip-CreER mice, and Q. Yang (University of Alabama, Birmingham, AL, USA) for providing the pCAG-CAT-X vector.

Data availability All data generated or analysed during this study are included in this published article (and its ESM files).

Funding This study was supported by the National Natural Science Foundation of China (81530024, 9174920038, 81471046, 81470988, 81670729 and 81401268), the Ministry of Science and Technology (2016YFC1305002, 2017YFC1309603 and 2017ZX09304022-007), the Integrated Innovative Team for Major Human Disease Programs of Tongji Medical College, Huazhong University of Science and Technology and the Innovative Funding for Translational Research from Tongji Hospital to CYW, and Horizon 2020 Program (T2D systems; GA667191) to DLE.

Duality of interest The authors declare that there is no duality of interest associated with this manuscript.

Contribution statement CYW conceived the project. XH, QL, CC, NL, FS, WH, SZ and PY contributed to the acquisition of data, analysis and interpretation. XH wrote the manuscript. CYW, SZ, QY and FX were involved in designing the strategy to generate and genotype the *Ubc9*$^{\Delta beta}$ and *Ubc9*^{Tg} mouse lines. SZ, ZC, QG, BR, JW, DLE and ZZ contributed to analysis and interpretation of the data. CYW, DLE and ZZ contributed to the study design and manuscript preparation. All authors were involved in drafting the article or revising it critically, and all authors gave their approval for the final manuscript to be published. CYW is the guarantor of this work and takes full responsibility for the content of the manuscript.

References

1. Yang P, Hu S, Yang F et al (2014) Sumoylation modulates oxidative stress relevant to the viability and functionality of pancreatic beta cells. Am J Transl Res 6:353–360
2. Flotho A, Melchior F (2013) Sumoylation: a regulatory protein modification in health and disease. Annu Rev Biochem 82:357–385
3. Li M, Guo D, Isales CM et al (2005) SUMO wrestling with type 1 diabetes. J Mol Med (Berlin, Germany) 83:504–513
4. Hajmrle C, Ferdaoussi M, Plummer G et al (2014) SUMOylation protects against IL-1beta-induced apoptosis in INS-1 832/13 cells and human islets. Am J Phys Endocrinol Metab 307:E664–E673
5. Pandey D, Chen F, Patel A et al (2011) SUMO1 negatively regulates reactive oxygen species production from NADPH oxidases. Arterioscler Thromb Vasc Biol 31:1634–1642
6. Guo D, Han J, Adam BL et al (2005) Proteomic analysis of SUMO4 substrates in HEK293 cells under serum starvation-induced stress. Biochem Biophys Res Commun 337:1308–1318
7. Kishi A, Nakamura T, Nishio Y, Maegawa H, Kashiwagi A (2003) Sumoylation of Pdx1 is associated with its nuclear localization and insulin gene activation. Am J Phys Endocrinol Metab 284:E830–E840
8. Mziaut H, Trajkovski M, Kersting S et al (2006) Synergy of glucose and growth hormone signalling in islet cells through ICA512 and STAT5. Nat Cell Biol 8:435–445
9. Shao C, Cobb MH (2009) Sumoylation regulates the transcriptional activity of MafA in pancreatic beta cells. J Biol Chem 284:3117–3124
10. Dai XQ, Kolic J, Marchi P, Sipione S, Macdonald PE (2009) SUMOylation regulates Kv2.1 and modulates pancreatic beta-cell excitability. J Cell Sci 122:775–779
11. Dai XQ, Plummer G, Casimir M et al (2011) SUMOylation regulates insulin exocytosis downstream of secretory granule docking in rodents and humans. Diabetes 60:838–847
12. Aukrust I, Bjorkhaug L, Negahdar M et al (2013) SUMOylation of pancreatic glucokinase regulates its cellular stability and activity. J Biol Chem 288:5951–5962
13. Ferdaoussi M, Dai X, Jensen MV et al (2015) Isocitrate-to-SENP1 signaling amplifies insulin secretion and rescues dysfunctional beta cells. J Clin Investig 125:3847–3860
14. Rajan S, Torres J, Thompson MS, Philipson LH (2012) SUMO downregulates GLP-1-stimulated cAMP generation and insulin secretion. Am J Phys Endocrinol Metab 302:E714–E723
15. Rajan S, Dickson LM, Mathew E et al (2015) Chronic hyperglycemia downregulates GLP-1 receptor signaling in pancreatic beta-cells via protein kinase A. Mol Metab 4:265–276
16. Ferdaoussi M, Fu J, Dai X et al (2017) SUMOylation and calcium control syntaxin-1A and secretagogin sequestration by tomosyn to regulate insulin exocytosis in human β cells. Sci Rep 7:248
17. Chen L, Fan C, Zhang Y et al (2013) Beneficial effects of inhibition of soluble epoxide hydrolase on glucose homeostasis and islet damage in a streptozotocin-induced diabetic mouse model. Prostaglandins & Other Lipid Mediators 104–105:42–48
18. Cheng J, Song J, He X et al (2016) Loss of Mbd2 protects mice against high fat diet-induced obesity and insulin resistance by regulating the homeostasis of energy storage and expenditure. Diabetes 65:3384–3395
19. Yang P, Li M, Guo D et al (2008) Comparative analysis of the islet proteome between NOD/Lt and ALR/Lt mice. Ann N Y Acad Sci 1150:68–71
20. He L, Sun F, Wang Y et al (2016) HMGB1 exacerbates bronchiolitis obliterans syndrome via RAGE/NF-kappaB/HPSE signaling to enhance latent TGF-beta release from ECM. Am J Transl Res 8:1971–1984
21. Han J, Zhong J, Wei W et al (2008) Extracellular high-mobility group box 1 acts as an innate immune mediator to enhance autoimmune progression and diabetes onset in NOD mice. Diabetes 57:2118–2127
22. Ran L, Yu Q, Zhang S et al (2015) Cx3cr1 deficiency in mice attenuates hepatic granuloma formation during acute schistosomiasis by enhancing the M2-type polarization of macrophages. Dis Model Mech 8:691–700
23. Wang J, Wei Q, Wang CY, Hill WD, Hess DC, Dong Z (2004) Minocycline up-regulates Bcl-2 and protects against cell death in mitochondria. J Biol Chem 279:19948–19954
24. Zhang M, Guo Y, Fu H et al (2015) Chop deficiency prevents UUO-induced renal fibrosis by attenuating fibrotic signals originated from Hmgb1/TLR4/NFkappaB/IL-1beta signaling. Cell Death Dis 6:e1847
25. Yao Y, Wang Y, Zhang Z et al (2016) Chop deficiency protects mice against bleomycin-induced pulmonary fibrosis by attenuating M2 macrophage production. Mol Ther J Am Soc Gene Ther 24:915–925
26. Hu S, Zhang Y, Zhang M et al (2015) Aloperine protects mice against ischemia reperfusion (IR)-induced renal injury by regulating PI3K/AKT/mTOR signaling and AP-1 activity. Mol Med. https://doi.org/10.2119/molmed.2015.00056
27. Liang H, Yin B, Zhang H et al (2008) Blockade of tumor necrosis factor (TNF) receptor type 1-mediated TNF-alpha signaling protected Wistar rats from diet-induced obesity and insulin resistance. Endocrinology 149:2943–2951
28. Jakobs A, Koehnke J, Himstedt F et al (2007) Ubc9 fusion-directed SUMOylation (UFDS): a method to analyze function of protein SUMOylation. Nat Methods 4:245–250
29. Wei W, Yang P, Pang J et al (2008) A stress-dependent SUMO4 sumoylation of its substrate proteins. Biochem Biophys Res Commun 375:454–459
30. Wang CY, Yang P, Li M, Gong F (2009) Characterization of a negative feedback network between SUMO4 expression and NFkappaB transcriptional activity. Biochem Biophys Res Commun 381:477–481
31. Pi J, Collins S (2010) Reactive oxygen species and uncoupling protein 2 in pancreatic beta-cell function. Diabetes Obes Metab 12(Suppl 2):141–148
32. Lei XG, Vatamaniuk MZ (2011) Two tales of antioxidant enzymes on beta cells and diabetes. Antioxid Redox Signal 14:489–503
33. Bhakkiyalakshmi E, Shalini D, Sekar TV, Rajaguru P, Paulmurugan R, Ramkumar KM (2014) Therapeutic potential of pterostilbene against pancreatic beta-cell apoptosis mediated through Nrf2. Br J Pharmacol 171:1747–1757
34. Yagishita Y, Fukutomi T, Sugawara A et al (2014) Nrf2 protects pancreatic beta-cells from oxidative and nitrosative stress in diabetic model mice. Diabetes 63:605–618
35. Cunha DA, Cito M, Carlsson PO et al (2016) Thrombospondin 1 protects pancreatic beta-cells from lipotoxicity via the PERK-NRF2 pathway. Cell Death Differ 23:1995–2006

36. Ramani K, Tomasi ML, Yang H, Ko K, Lu SC (2012) Mechanism and significance of changes in glutamate-cysteine ligase expression during hepatic fibrogenesis. J Biol Chem 287:36341–36355
37. Lau A, Tian W, Whitman SA, Zhang DD (2013) The predicted molecular weight of Nrf2: it is what it is not. Antioxid Redox Signal 18:91–93
38. Hourihan JM, Moronetti Mazzeo LE, Fernandez-Cardenas LP, Blackwell TK (2016) Cysteine sulfenylation directs IRE-1 to activate the SKN-1/Nrf2 antioxidant response. Mol Cell 63:553–566
39. Ngo HKC, Kim DH, Cha YN, Na HK, Surh YJ (2017) Nrf2 mutagenic activation drives hepatocarcinogenesis. Cancer Res 77: 4797–4808
40. Soares MA, Cohen OD, Low YC et al (2016) Restoration of Nrf2 signaling normalizes the regenerative niche. Diabetes 65:633–646
41. Saito T, Ichimura Y, Taguchi K et al (2016) p62/Sqstm1 promotes malignancy of HCV-positive hepatocellular carcinoma through Nrf2-dependent metabolic reprogramming. 7:12030
42. Rabbani PS, Zhou A, Borab ZM et al (2017) Novel lipoproteoplex delivers Keap1 siRNA based gene therapy to accelerate diabetic wound healing. Biomaterials 132:1–15
43. Hayes JD, Dinkova-Kostova AT (2014) The Nrf2 regulatory network provides an interface between redox and intermediary metabolism. Trends Biochem Sci 39:199–218
44. Itoh K, Wakabayashi N, Katoh Y et al (1999) Keap1 represses nuclear activation of antioxidant responsive elements by Nrf2 through binding to the amino-terminal Neh2 domain. Genes Dev 13:76
45. Uruno A, Furusawa Y, Yagishita Y et al (2013) The Keap1-Nrf2 system prevents onset of diabetes mellitus. Mol Cell Biol 33:2996–3010